



OPEN Chronic NH₄Cl loading improves glucose tolerance without modifying insulin sensitivity in mice

Nawel Zaibi^{1,2,✉}, Jessica Montaigne², Jennifer Baraka-Vidot^{1,5}, Judith Merrheim^{1,5}, Claire Devos^{1,5}, Emilie Caron³, Florent Auger², Emmanuelle Durand¹, Bénédicte Toussaint^{1,2}, Souhila Amanzougarene^{1,2}, Mehdi Derhourhi^{1,2}, Philippe Froguel^{1,2,4}, Amélie Bonnefond^{1,2,4,6}, Régine Chambrey^{1,6} & Christophe Breton^{1,2,6,✉}

Acute metabolic acidosis (MA), a feature mostly associated with chronic kidney disease, decreases glucose tolerance and insulin sensitivity. By contrast, the effects of chronic MA on glucose homeostasis remain elusive. Here, we evaluated glucose homeostasis and metabolic parameters in male mice exhibiting chronic MA via long-term NH₄Cl administration. Unlike acute MA, chronic MA resulted in lower body weight, increased energy expenditure, lower basal glycemia, improved glucose tolerance without changes in insulin secretion or sensitivity. No overall glucose uptake changes were observed. However, hepatic and intestinal gluconeogenesis were decreased whereas renal endogenous glucose production was increased in mice with chronic MA. The elevated glucose urinary excretion was associated with lower expression of renal sodium/glucose co-transporters. Transcriptomic analysis revealed that chronic MA potentiates anion transport, glucose and lipid metabolism, mitochondrial and oxidative phosphorylation pathways in the kidney. Overall, chronic MA improves glucose tolerance without changes in insulin secretion or sensitivity, likely due to reduced hepatic gluconeogenesis, decreased renal glucose reabsorption and increased energy demands in the kidney.

Keywords Gene expression, Gluconeogenesis, Glucose homeostasis, Metabolic parameters, pH regulation, Renal function

The global incidence of chronic kidney disease (CKD) which involves a gradual loss of kidney functions, has reached a considerable number over the past years¹, along with its complications. Acute metabolic acidosis (MA) is well known to be associated with CKD², although few of these patients receive therapy to correct the pH imbalance³. Additionally, MA has been shown to lead to insulin resistance and/or impaired glucose homeostasis^{4–8}, decreasing further the quality of life of patients.

Indeed, MA most commonly develops as CKD progresses due to a reduced acid excretion capacity and/or high daily exogenous acid load, resulting in a positive H⁺ balance⁹. As the number of viable nephrons decreases during disease progression¹⁰, single nephron acid excretion, especially via ammoniogenesis improves in some cases despite the reduced net renal acid excretion¹¹. Single nephron acid excretion is enhanced, but not enough to compensate for the daily acid load, leading to a lost acid base balance⁵ and reduced bicarbonate concentration¹². Serum bicarbonate concentration reduction has been associated with impaired fasting glucose and a higher risk of type 2 diabetes (T2D) in patients¹³. Ammonium chloride (NH₄Cl) administration in healthy dogs demonstrated the impact of acute MA on decreased glucose uptake, causing chronic hyperglycemia linked to insulin resistance^{14–16}. In healthy individuals, NH₄Cl treatment led to insulin resistance after only 3 days of treatment^{17,18}, which could partially be due to impaired insulin signaling via phosphoinositide 3-kinase (PI3K) in the muscle¹⁹, potentially associated with increased proteolysis, known to occur during MA²⁰. Furthermore, acute MA led to decreased insulin receptors in adipocytes²¹, and decreased plasma adiponectin and leptin levels^{22,23}. In line with these findings, the correction of MA by sodium bicarbonate (NaHCO₃) supplementation in CKD patients not only decreased the progression of kidney failure, but reduced plasma insulin concentration

¹Inserm UMR1283, CNRS UMR8199, European Genomic Institute for Diabetes (EGID), Institut Pasteur de Lille, Lille University Hospital, Lille, France. ²Université de Lille, Lille, France. ³Université de Lille, Inserm, CHU Lille, U1172 LiNCog-Lille Neuroscience & Cognition, Lille, France. ⁴Department of Metabolism, Imperial College London, London, UK. ⁵These authors contributed equally: Jennifer Baraka-Vidot, Judith Merrheim and Claire Devos. ⁶These authors jointly supervised this work: Amélie Bonnefond, Régine Chambrey and Christophe Breton. ✉email: nawel.zaibi@univ-lille.fr; christophe.breton@univ-lille.fr

and lowered the need for anti-diabetic drugs⁷, showing a clear relationship between blood pH and glucose homeostasis.

Over the past years, most functional studies have assessed the effects of acute MA^{14,18–24}. By contrast, the effects of chronic MA on glucose tolerance and insulin resistance remain elusive. Questioning the effects of chronic MA in animal models may provide valuable information on underlying mechanisms resulting in glucose homeostasis deregulation and higher T2D risk in patients with long term acid–base balance disruption. Here, we evaluated metabolic parameters and glucose homeostasis in mice exhibiting chronic MA.

Results

Chronic NH₄Cl treatment induces MA

Treatment reduced blood pH and bicarbonate concentrations over the duration of the kinetic experiments (2-Way ANOVA, $P < 0.0001$) (Supplementary Fig. 1A,B). Chloride ion concentrations were higher in treated mice (2-Way ANOVA, $P < 0.0001$; Supplementary Fig. 1C). The pressure of carbon dioxide was lower in treated mice over the 180 days (2-Way ANOVA, $P = 0.0027$; Supplementary Fig. 1D). Blood sodium concentration was increased in treated mice (2-Way ANOVA, $P = 0.001$; Supplementary Fig. 1E). Blood potassium concentration, urea concentration and hematocrit remained unchanged following treatment (Supplementary Figs. 1F,G and H, respectively).

Chronic NH₄Cl treatment induces total body weight loss with an increase in energy expenditure

Control mice continuously gained weight over the duration of the study but MA mice reached a plateau after day 60 (2-Way ANOVA, $P < 0.0001$; Fig. 1A), despite having a higher food and liquid intake (2-Way ANOVA, $P < 0.0001$; Fig. 1B,C). Fat mass percentage over total body weight was higher in MA mice (2-Way ANOVA, $P = 0.011$; Fig. 1D), lean mass was lower compared to the control mice (2-Way ANOVA, $P < 0.0001$; Fig. 1E) and fluid mass was similar in both groups (Fig. 1F). Energy expenditure (EE) was overall higher in MA mice (2-Way ANOVA, $P = 0.036$; Fig. 1G).

Chronic NH₄Cl treatment increases glucose tolerance in mice without changes to both insulin secretion and insulin sensitivity

After 7 days of treatment, mice showed increased glucose tolerance *vs* controls (2-Way ANOVA, $P < 0.0001$; Fig. 2A). Blood glucose levels were lower in MA mice compared to controls after 45, 60 and 90 min (Šidák's multiple comparisons test, $P = 0.0029$, $P = 0.0025$ and $P = 0.0020$ respectively; Fig. 2A). The ameliorated glucose tolerance is also observed on the area under the curve (AUC) of MA mice *vs* controls (*t*-test, $P = 0.0097$; Fig. 2B). No differences in blood insulin levels were found in MA mice when compared to controls (2-Way ANOVA, $P = 0.33$; Fig. 2C).

The improved glucose tolerance was still observed after 120 days of treatment (2-Way ANOVA, $P = 0.0002$; Fig. 2D). Basal blood glucose levels were similar in both groups (Fig. 2D), as well as 15- and 30-min post glucose injection (Fig. 2D). Glycemia of acidotic mice reduced further than control mice's glycemia 30 min post-glucose injection (Fig. 2D). The AUC of blood glucose tended to be lower in MA mice (*t*-test, $P = 0.054$; Fig. 2E). Plasma insulin concentrations were similar in both groups (Fig. 2F).

After 15, 60, 90, 150 and 180 days of treatment, glucose tolerance was also improved in MA mice when compared to controls with no changes in insulin secretion (Supplementary Figs. 2A to 2O). Fasting glycemia of MA mice were lower compared to the controls throughout the study (2-Way ANOVA, $P < 0.0001$; Supplementary Fig. 3).

After 7 days of treatment, insulin tolerance was similar in both groups (Fig. 2G), as reflected by the respective AUCs (Fig. 2H). Fasting plasmatic insulin concentrations were comparable in both groups (Fig. 2I). Equivalent results were observed after 120 days of treatment (Fig. 2L). Fasting plasmatic insulin concentrations were alike in both groups after 15, 30, 60, 90, 150 and 180 days of treatment (Supplementary Figs. 4A to R).

Chronic NH₄Cl treatment alters gluconeogenesis in a tissue-specific manner

After 7 days of treatment, pyruvate induced endogenous glucose production (EGP) was similar in both groups (Fig. 3A) as shown in the corresponding AUC (Fig. 3B). Comparable results were observed after 15 (Supplementary Figs. 5A–C) and 30 days of treatment (Supplementary Figs. 5D–F). However, 60 days of treatment led to reduced gluconeogenesis *vs* controls (2-Way ANOVA, $P = 0.00030$; Supplementary Fig. 5G). This effect was even more pronounced after 90 days of treatment (2-Way ANOVA, $P < 0.0001$; Supplementary Fig. 5J). Blood glucose was lower in MA mice at 30 (*t*-test, $P = 0.022$ Supplementary Fig. 5J) and 60 min post-pyruvate injection (*t*-test, $P = 0.025$ Supplementary Fig. 5J), without differences in the AUC (Supplementary Fig. 5K). After 120 days of treatment, total gluconeogenesis was reduced in MA mice *vs* controls (2-Way ANOVA, $P = 0.025$; Fig. 3C), without changes of the AUC (Fig. 3D). After 150 and 180 days of treatment, no differences were observed between both groups (Supplementary Figs. 5M to R). No differences in insulin secretion were observed during the PTTs (data not shown).

Then, alanine (hepatic EGP substrate) and glutamine (renal and intestinal EGP substrate) stimulated gluconeogenesis tests were performed. MA mice had reduced hepatic EGP after 7 days (2-Way ANOVA, $P < 0.0001$; Fig. 3E), confirmed by the AUCs (*t*-test, $P = 0.041$; Fig. 3F). Hepatic EGP was also reduced in treated mice after 120 days (2-Way ANOVA, $P = 0.00040$; Fig. 3G), with no differences in the AUC (Fig. 3H). Reduced hepatic gluconeogenesis was not or barely observable after 30, 60 and 90 days of treatment (Supplementary Figs. 6). Chronic treatment also led to reduced renal/intestinal gluconeogenesis. From day 7 of the study, MA mice produced less glucose after glutamine injection *vs* controls (2-Way-ANOVA, $P = 0.0012$; Fig. 3I), without changes of the AUC (Fig. 3J). This was also the case after 30 and 60 days of treatment (2-Way ANOVA,

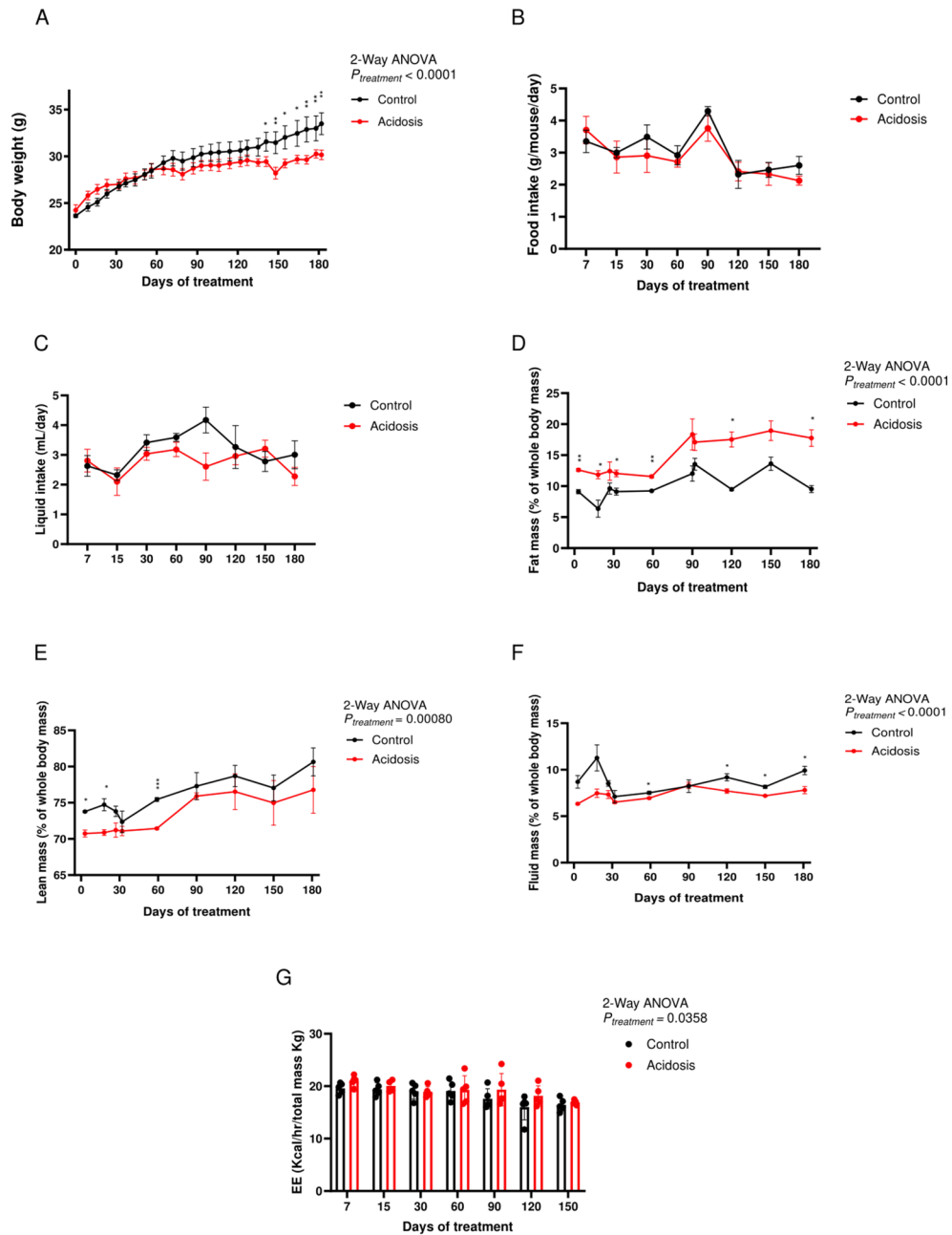


Fig. 1. Body composition and metabolic performances are altered in acidotic mice. (A) Body weight of control (black) and acidotic (red) mice on chow diet between 0 and 180 days of NH_4Cl treatment ($n=6$ per group). (B,C) Average food (B) and liquid intake (C) of control and acidotic mice between 0 and 180 days of NH_4Cl treatment ($n=6$ cages per group). (D–F) Percentage of fat (D), lean (E) and fluid (F) mass relative to the total body weight of control and acidotic mice between 0 and 180 days of NH_4Cl treatment ($n=6$ for the control and 5 for the acidotic mice). (G) Energy expenditure of control and acidotic mice between 7 and 150 days of NH_4Cl treatment. All values are expressed as mean \pm SEM. EE: energy expenditure, ns: not significant; Kcal: kilo calories.

$P < 0.0001$; Supplementary Figs. 7A,C). No effects were observed at 90 days of treatment between both groups (Supplementary Figs. 7E,F). However, 120 days of treatment led to a reduction of glutamine stimulated EGP vs controls (2-Way ANOVA, $P < 0.0001$; Fig. 3K). Glutamine derived EGP was lower in acidotic mice after 30-, 45-, 60- and 90-min post injection (Šidák's multiple comparison test, $P < 0.0001$, $P < 0.0001$, $P = 0.0030$ and $P = 0.0092$ respectively; Fig. 3K). The AUC of glycemia in MA mice was lower vs controls (t -test, $P = 0.0010$; Fig. 3L).

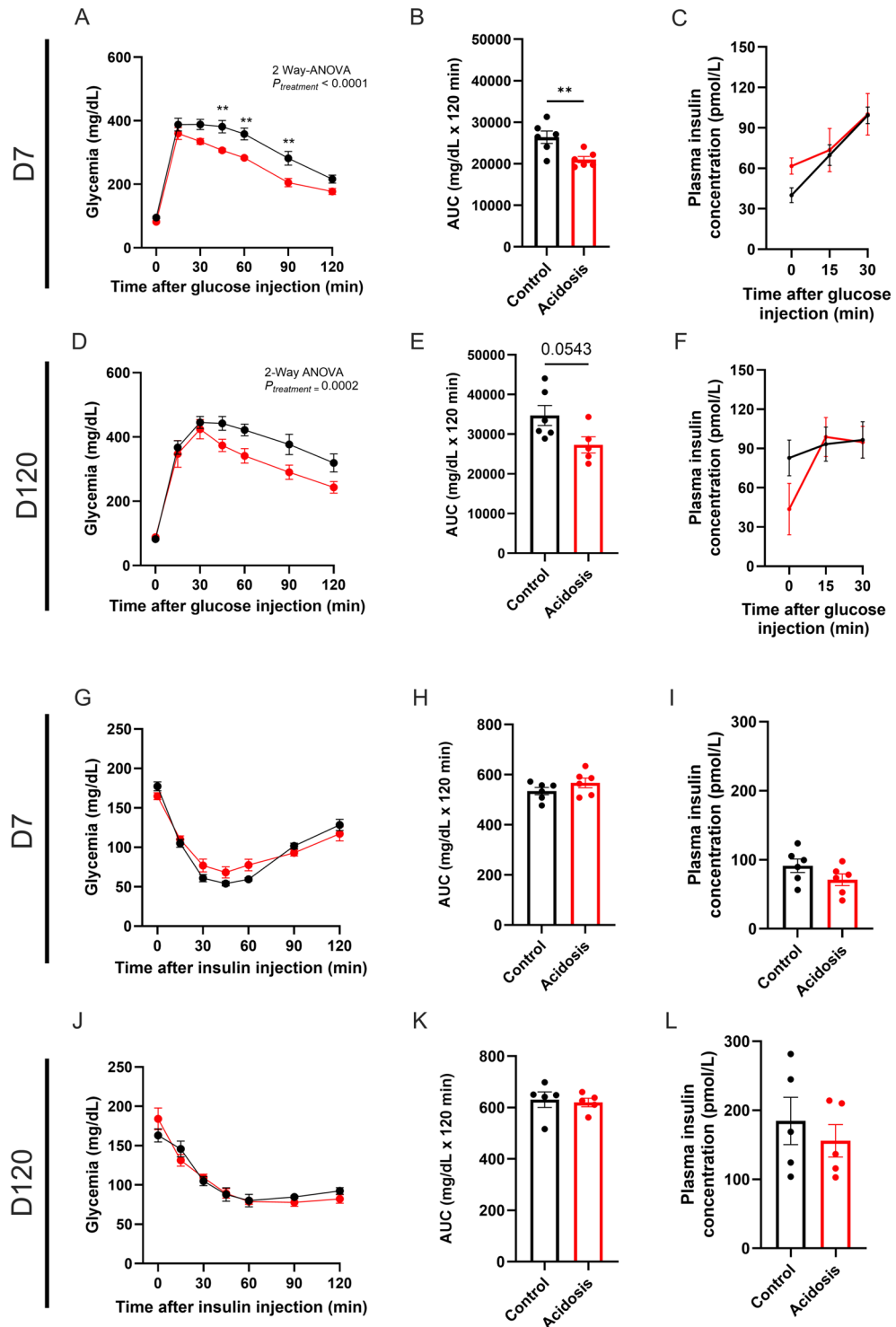


Fig. 2. Glucose tolerance is improved without changes of insulin secretion or sensitivity in acidotic mice. (A–C) Intraperitoneal glucose tolerance test (ipGTT) in control (black) and acidotic (red) mice after 7 days of NH_4Cl treatment ($n = 6$ per group) (A) with the corresponding area under the curve (AUC) with baseline values subtracted (B) and plasmatic insulin levels measured during ipGTT (C). (D–F) ipGTT in control and acidotic mice under chow diet after 120 days of NH_4Cl treatment ($n = 6$ for the control and 5 for the acidotic mice) (D) and the corresponding AUC with baseline values subtracted (E) and plasmatic insulin levels measured during ipGTT (F). (G–I) Intraperitoneal insulin tolerance test (ipITT) in control and acidotic mice after 7 days of NH_4Cl treatment ($n = 6$ per group) (G) and the corresponding AUC with baseline values subtracted (H) and basal plasmatic insulin levels measured during ipITT (I). (J–L) ipITT in control and acidotic mice after 120 days of NH_4Cl treatment ($n = 5$ per group) (J) and the corresponding AUC with baseline values subtracted (K) and basal plasmatic insulin levels measured during ipITT (L). All values are expressed as mean \pm SEM.

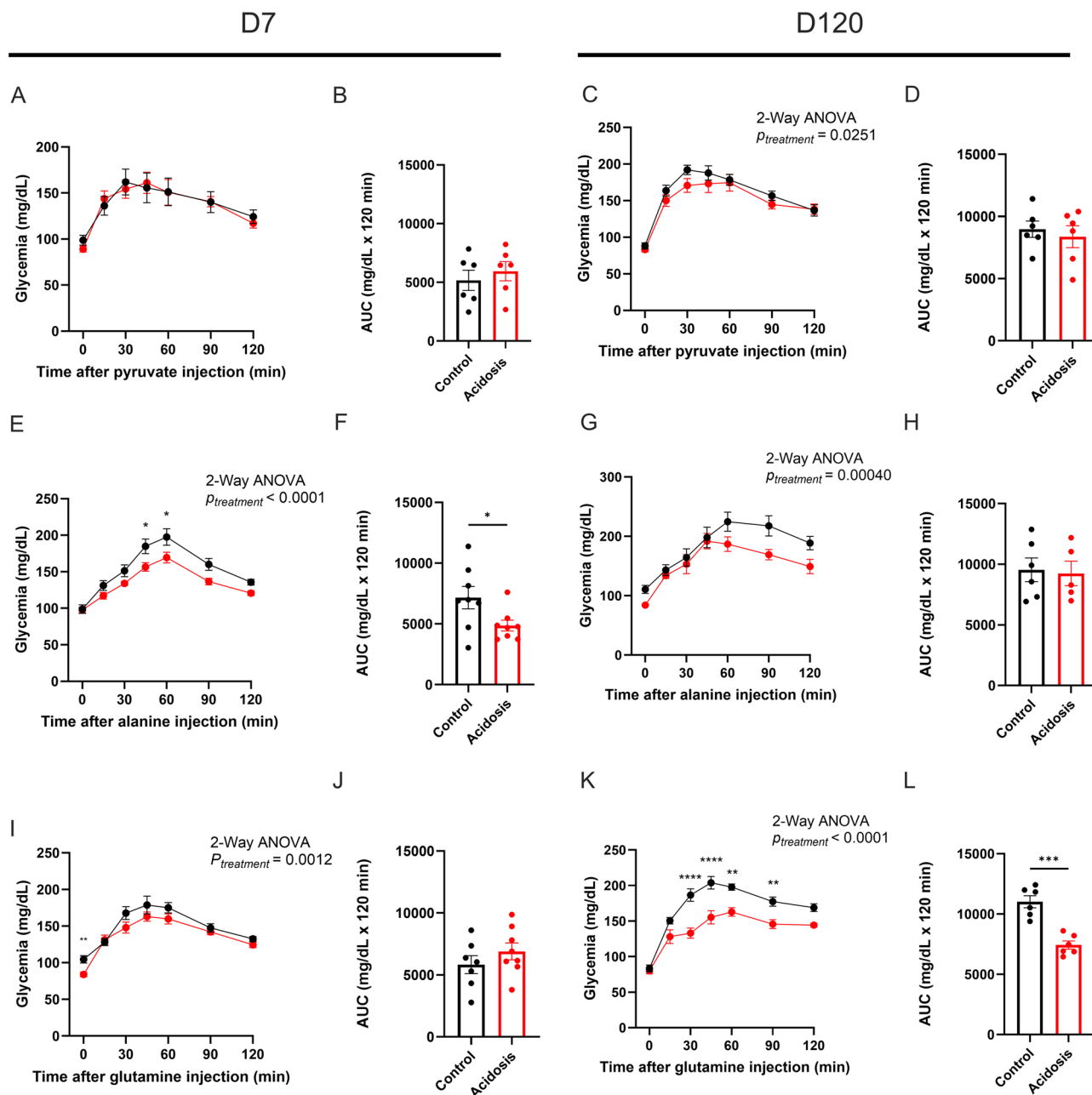
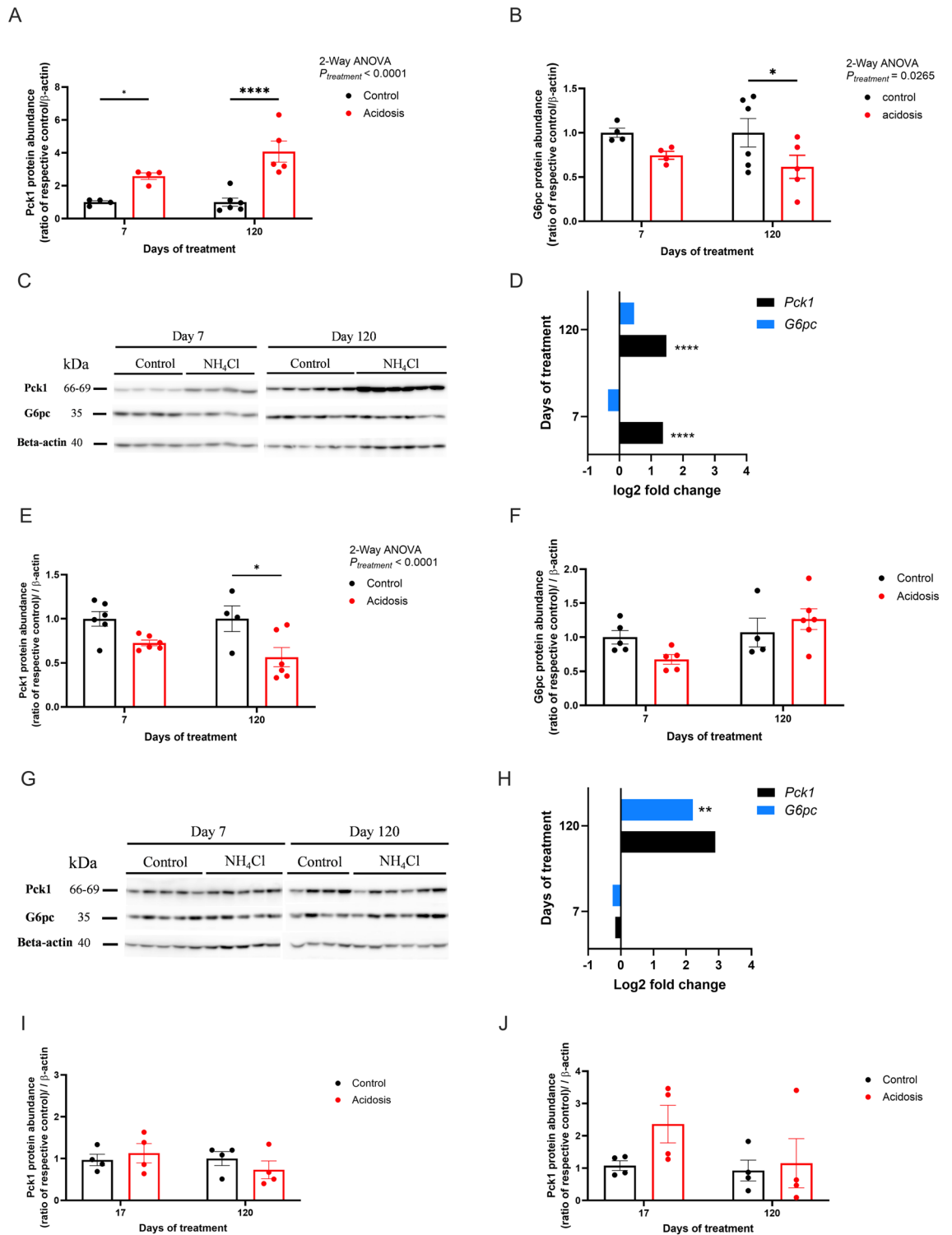


Fig. 3. Endogenous glucose production is reduced in acidotic mice. (A,B) Intraperitoneal pyruvate tolerance test (ipPTT) in control (black) and acidotic (red) mice after 7 days of NH_4Cl treatment ($n=6$ per group) with the corresponding area under the curve (AUC) of ipPTT with baseline values subtracted (B). (C,D) ipPTT in control and acidotic mice after 120 days of NH_4Cl treatment ($n=6$ per group) (C) and the AUC with baseline values subtracted (D) of ipPTT. (E,F) Intraperitoneal alanine tolerance test (ipAlaTT) (E) in control (black) and acidotic (red) mice after 7 days of NH_4Cl treatment ($n=8$ per group) and the corresponding AUC with baseline values subtracted (F). (G,H) IpAlaTT in control and acidotic mice under chow diet after 120 days of NH_4Cl treatment ($n=6$ for the control and 5 for the acidotic mice) (G) and the corresponding AUC with baseline values subtracted (H). (I,J) Intraperitoneal glutamine tolerance test (ipGluTT) in control (black) and acidotic (red) mice under chow diet after 7 days of NH_4Cl treatment ($n=7$ for the control and 8 for the acidotic mice) (I) and the corresponding AUC with baseline values subtracted (J). (K,L) ipGluTT in control and acidotic mice under chow diet after 120 days of NH_4Cl treatment ($n=6$ per group) (K) with the AUC of ipPTT (L). All values are expressed as mean \pm SEM.

Chronic NH_4Cl treatment increases the expression of key actors regulating renal and intestinal gluconeogenesis and decreases the expression of those involved in hepatic gluconeogenesis

To analyze further the effects of chronic MA on tissue specific gluconeogenesis, protein and RNA expression of



Pck1/Pck1 and *G6pc/G6pc* were assessed in the kidney, the liver, the duodenum and the jejunum²⁵. Renal *Pck1* protein expression was increased by the treatment (2-Way ANOVA, $P < 0.0001$; Fig. 4A,C and Supplementary Fig. 11) whereas *G6pc* expression was reduced only in the later stages of the kinetic study (2-Way ANOVA, $P = 0.026$; 120 days of treatment $P = 0.038$; Fig. 4B,C and Supplementary Fig. 11). RNA expression analysis showed a marked upregulation on renal *Pck1* throughout the study (Fig. 4D) and no significant difference of *G6pc* renal expression (Fig. 4D). Hepatic *Pck1* expression reduced at the latter stages of the study (2-Way ANOVA, $P < 0.0001$; 120 days of treatment $P = 0.012$; Fig. 4E and Supplementary Fig. 12), but no differences were observed at the early stages of the study (Fig. 4E,G and Supplementary Fig. 12). Chronic MA did not alter hepatic *G6pc* expression (Fig. 4F,G and Supplementary Fig. 12). mRNA expression of both *Pck1* and *G6pc* was increased in the liver in treated animals compared to their controls (2-Way ANOVA, $P < 0.0001$ and $P = 0.00090$ respectively; Fig. 4H). Duodenal and jejunal *Pck1* expression were not altered after 17 and 120 days of treatment (Fig. 4I,J). RNA-seq showed that the renal expression of *Pcx* (pyruvate carboxylase), *Pck1* (phosphoenolpyruvate

◀ **Fig. 4.** The expression of key actors of hepatic and extra hepatic gluconeogenesis is altered in a tissue specific manner in acidotic mice. (A–C) Quantification of *Pck1* (A) and *G6pc* (B) from a Western Blot assay (C) showing protein levels in kidney lysates of control (black) and acidotic (red) mice ($n=4$ per group at day 7 and 6 at day 120) Beta-actin was used as a loading control. Quantification was performed using the ImageQuant software. (D) Log₂ fold change of mRNA expression of *Pck1* and *G6pc* in the kidney of control and acidotic mice after 7 and 120 days of treatment ($n=4$ per group). (E–G) Quantification of *Pck1* (E) and *G6pc* (F) from a Western Blot assay (G) showing protein levels in liver lysates of control (black) and acidotic (red) mice ($n=5$ at day 7 and 4 for the control and 6 for the NH_4Cl at day 120) Beta-actin was used as a loading control. Quantification was performed using the ImageQuant software. (H) Log₂ fold change of mRNA expression of *Pck1* and *G6pc* in the liver of control and acidotic mice after 7 and 120 days of treatment ($n=4$ per group). (I, J) Quantification of PCK1 in the duodenum (J) and jejunum (K) from a Western Blot assay showing protein levels of control and acidotic mice after 17 and 120 days of treatment ($n=4$ per group); beta-actin was used as a loading control. All blots have been cropped for presentation purposes and original blots are presented in Supplementary Figs. 11 and 12. Quantification was performed using the ImageQuant software. All values are expressed as mean \pm SEM except for the Log₂ fold change values.

carboxykinase 1, cytosolic), *Fbp1* (fructose-bisphosphatase 1), *Fbp2* (fructose-bisphosphatase 2) and *G6pc* (glucose-6-phosphatase) was altered between 3 and 60 days of treatment (Supplementary Fig. 8).

Increased glucose urinary excretion is associated with lower expression of renal sodium/ glucose co-transporters in acidotic mice

Glucose homeostasis is regulated by endogenous glucose production/breakdown, glucose renal clearance and glucose uptake/storage^{24–26}. We therefore assessed renal excretion of glucose in MA mice by measuring glucose excretion 4 h after an oral glucose bolus. MA mice showed an increase in glucosuria vs control mice after 7, 30 (Sidak's multiple comparison test, $P=0.031$ and $P=0.035$ respectively; data not shown), and 90 days of treatment (Sidak's multiple comparison test, $P=0.0076$; Fig. 5A).

The expression of renal glucose transporters, located in the proximal tubule, was therefore investigated. *Slc5a2* (*Sglt2*) mRNA of treated mice was downregulated compared to control mice after short and long terms of the kinetic study (J7, $P=0.0098$; J120, $P=0.0013$, Fig. 5B). Expression of *Slc5a1* (*Sglt1*) mRNA was upregulated in acidotic mice compared to their control at short terms of the kinetic study (J7, $P=0.00053$, Fig. 5B). mRNA expression of both *Slc2a2* (*Glut2*) and *Slc2a1* (*Glut1*) were not altered by the treatment (Fig. 5B).

Protein expression of both sodium glucose co-transporters were not altered by the NH_4Cl load after 7 days, but were significantly reduced over 120 days (Sidak's multiple comparison test, $P=0.030$ and $P=0.047$; Fig. 5C,D respectively and Fig. 5G and Supplementary Fig. 13). *Glut2* expression was not altered by the treatment after 7 days, but its protein expression was significantly upregulated after 120 days (Sidak's multiple comparison test, $P=0.0012$, Fig. 5E,G and Supplementary Fig. 13). *Glut1* renal expression was not altered by NH_4Cl load (Fig. 5F,G and Supplementary Fig. 13).

Chronic MA does not alter whole body 2-deoxy-2-[18F] fluoroglucose uptake but increases glucose uptake in kidney and bladder

Following the 2-Deoxy-2-[18F] fluoroglucose (¹⁸FDG) injection after 180 days of NH_4Cl load, whole-body standard uptake value (SUV) was similar in both groups (Fig. 6A). This was also observed at the tissue level in muscle, inguinal white adipose tissue, perigonadal white adipose tissue, brown adipose tissue and brain (Supplementary Figs. 9A to E). However, MA mice displayed an increase in ¹⁸FDG SUV in the kidney (~1.5-fold) and bladder (~twofold) (unpaired *t*-test, $P=0.026$ and $P=0.017$, respectively; Fig. 6B–E).

Chronic MA potentiates anion transport, glucose and lipid metabolism, mitochondrial and oxidative phosphorylation pathways in the kidney

To decipher altered mechanisms in response to chronic MA, transcriptomic analysis of whole kidney was determined by RNA-seq between 3 and 60 days of treatment (Supplementary Table 3 and Supplementary Fig. 10). 70 genes were differentially expressed (30 up-regulated and 40 down-regulated) after 7 days of treatment (Fig. 7A). Sequencing analysis revealed a strong enrichment of upregulated genes in the anion transport pathway (such as *Best1*, *Slc13a2*, *Slc38a3*, *Slc13a4*, *Slc26a6*, *Slc25a25*, *Abca17*, *Lcn2*, *Fabp5* and *Cox6a2*; Fig. 7C and Supplementary Table 1). A marked activation of glucuronic metabolism (i.e., up-regulation of *Dcxr*, *Ugt1a1*, *Ugt1a3*, *Gstm5*, *Nat8*, *Rarres2*, *Pck1*, *Ptgds*, *Bace2* and *Abca1*; Fig. 7B,C and Supplementary Table 1) and glucose metabolism was observed (i.e., up-regulation of *Fabp5*, *Pck1*, *Dcxr*, *Abca1*, *Ptgds*, *Mogat2*, *Fitm1*, *Phospho1* and *Bace2*; Fig. 7B,C and Supplementary Table 1). NH_4Cl loading had an inhibitory effect on renal secretion regulation (i.e., down-regulation of *Ces1g*, *Cyp27b1*, *Irs1*, *Septin2*, *Syt7*, *Exph5*, *Zbed6* and *Prr5l*; Fig. 7B,D and Supplementary Table 1).

101 genes were differentially expressed (55 up-regulated and 46 down-regulated; Fig. 8A) after 60 days of treatment. Proximal tubule bicarbonate reclamation, cellular response to pH and anion transport were still upregulated in treated mice (i.e., up-regulation of *Gls*, *Glud1*, *Pck1*, *Slc38a3*, *Slc34a2*, *Slc16a14*, *Slc16a6*, *Slc26a7*, *Slc26a10*, *Slc4a7* and *Slc10a5*; Fig. 8B,C and Supplementary Table 1). Activation of the negative regulation of leukocyte migration (i.e., up-regulation of *Grem1*, *Ccl28*, *Mmp28*, *Atp7a*, *Loxl4* and *Papln*; Fig. 8C and Supplementary Table 1) and increased regulation of glucose metabolism (i.e., up-regulation of *Irs1*, *Sorbs1*, *Dgkq* and *Pdk1*; Fig. 8A–C and Supplementary Table 1) were also observed. Chronic NH_4Cl loading inhibited the complement cascade (i.e., down-regulation of *C2*, *Cfi*, *F2*, *Masp2* and *Igkc*; Fig. 8A,B,D and Supplementary Table

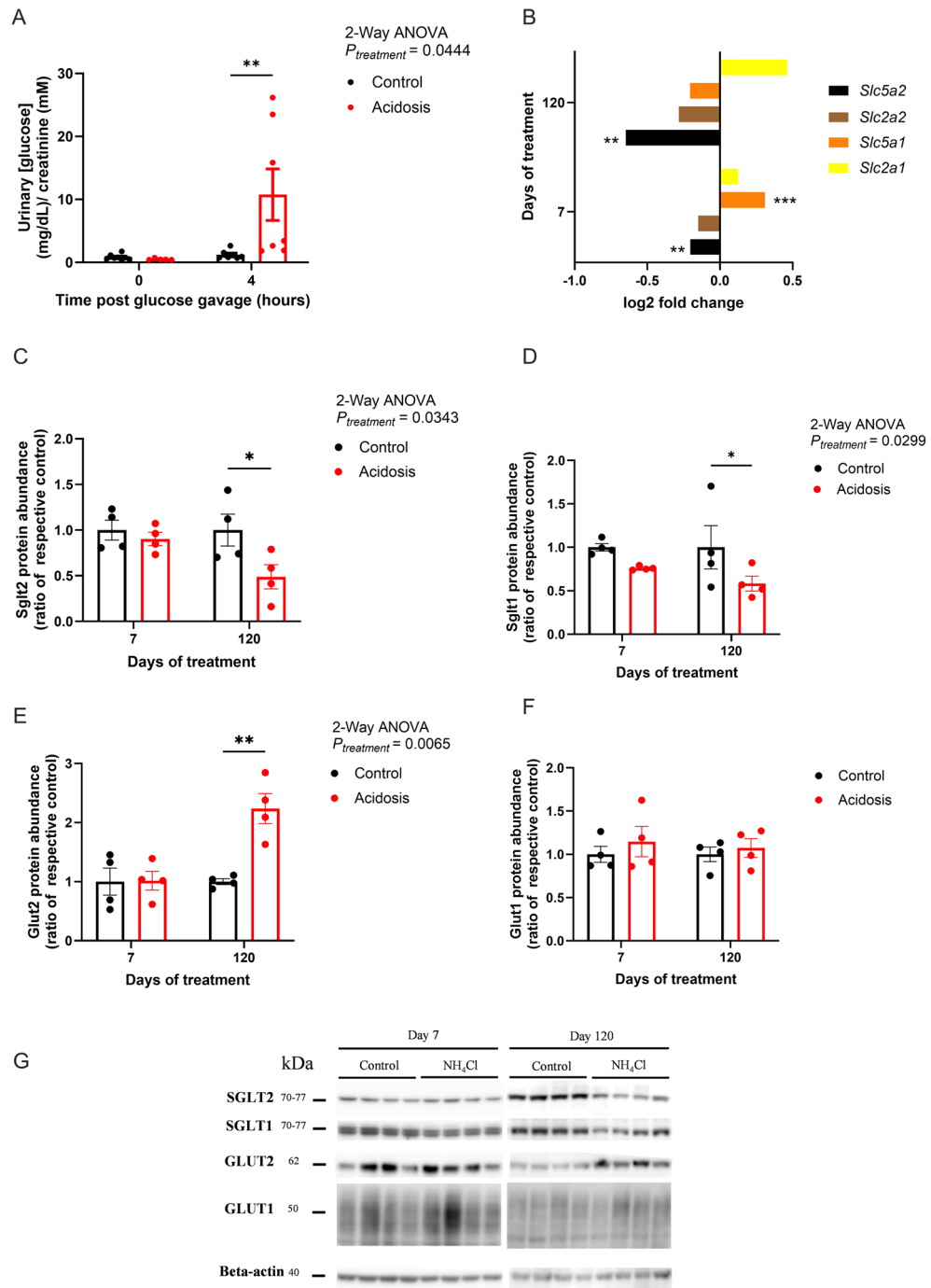


Fig. 5. Increased glucose urinary excretion is associated with lower expression of renal sodium/glucose co-transporters in acidotic mice. **(A)** Urinary glucose concentration before and after an oral bolus of 2 g/kg of body weight in control mice (black) and mice treated for 90 days (red) (T0, $n = 8$ for the control and 5 for the acidotic mice. T4, $n = 7$ per group). **(B)** Log₂ fold change of mRNA expression of *Slc5a2*, *Slc2a2*, *Slc5a1*, and *Slc2a1* in the kidney of control and acidotic mice after 7 and 120 days of treatment ($n = 4$ per group). **(C–G)** Quantification of SglT2 **(C)**, SglT1 **(D)**, Glut2 **(E)** and Glut1 **(F)** from a Western Blot assay **(G)** showing protein levels in kidney of control (black) and acidotic (red) mice ($n = 4$ per group). Beta-actin was used as a loading control. All blots have been cropped for presentation purposes and original blots are presented in Supplementary Fig. 13. Quantification was performed using the ImageQuant software. **(G)** All values are expressed as mean \pm SEM except for the Log₂ fold change values.

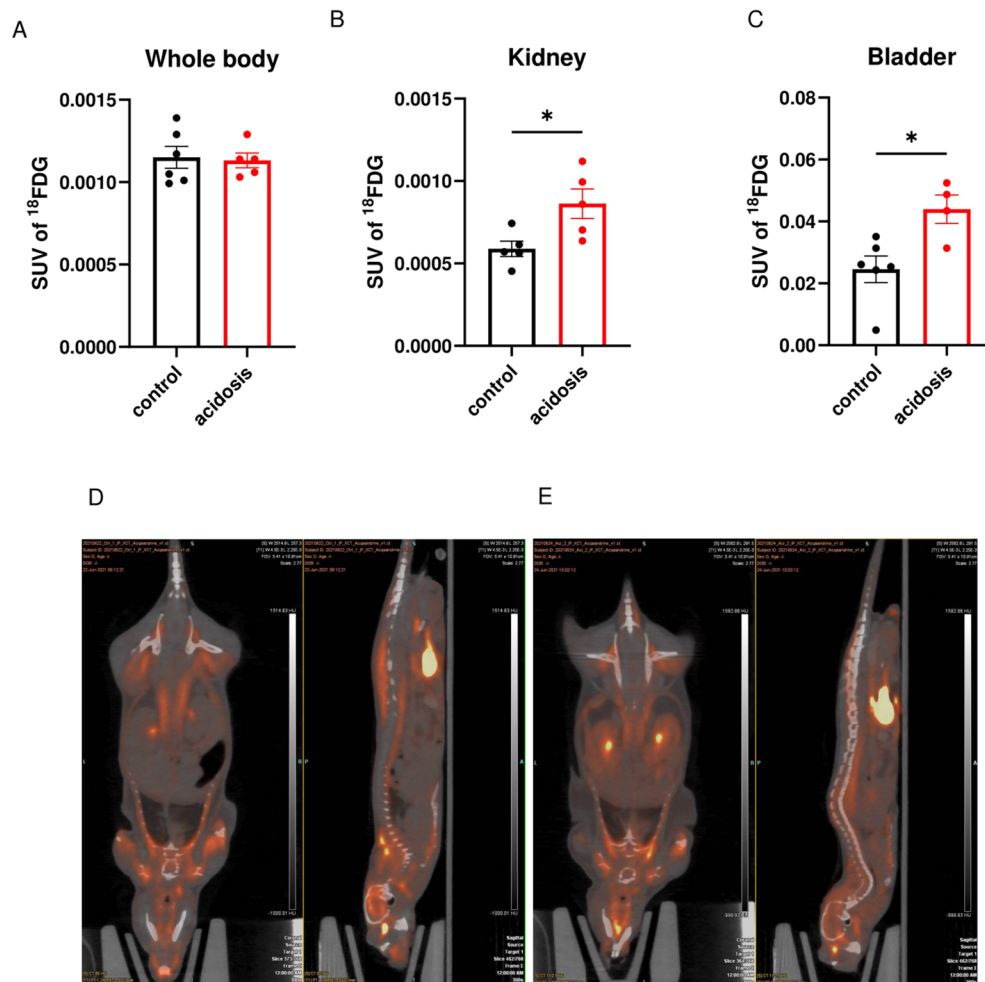


Fig. 6. 180 days of NH_4Cl treatment does not alter whole body 2-Deoxy-2-[^{18}F]fluoroglucose uptake but increases glucose uptake in kidney and bladder. (**A–C**) Standard uptake values (SUV) of 2-Deoxy-2-[^{18}F]fluoroglucose (^{18}F FDG) in the whole body (**A**), kidney (**B**) and bladder (**C**) of control (black) and acidotic (red) mice under chow diet after 180 days of NH_4Cl treatment ($n=6$ for the control and 5 for the acidotic mice). (**D,E**) Positron emission tomography (PET) scan of a control (**D**) and acidotic mouse (**E**) after injection of ^{18}F FDG. All values are expressed as mean \pm SEM. SUV standard uptake value.

1) and downregulated genes involved in the cytochrome P450 mechanism (i.e., *Cyp24a1*, *Cyp27b1*, *Cyp4b1*, *Tbxas1*, *Inmt*, *Miox* and *Slc34a3*; Fig. 8A,B,D and Supplementary Table 1).

Discussion

Acute MA has been linked to glucose intolerance via insulin resistance in both animals and humans^{14–19}. In this study, chronic MA by NH_4Cl loading produced marked and sustained effects on energy metabolism, glucose homeostasis, and renal function. The reduction in blood pH, bicarbonate concentration accompanied by elevated plasma chloride, confirm the establishment of chronic MA. These biochemical changes are in line with previous observations in NH_4Cl -loaded models and validate the use of this approach to mimic acidotic states in vivo^{27–29}. A striking outcome of chronic MA was the divergence between similar food and drink intake and the attenuation of body weight gain. Despite similar energy intake, treated mice displayed increased energy expenditure, reduced lean mass, and increased fat distribution. These results suggest that acidosis imposes a metabolic cost that impairs anabolic processes, as protein breakdown is accelerated to supply renal ammoniogenesis with substrates such as glutamine²⁰.

Strikingly, chronic MA improved glucose tolerance, without altering insulin secretion or overall sensitivity, suggesting enhanced non-insulin-mediated glucose disposal, previously reported by Mannon et al.³⁰ in Sprague-Dawley rats with a 7 days NH_4Cl load. It is important to note that, as mentioned earlier, acidotic mice displayed a reduced lean mass compared to controls and therefore, could have a tissue dependent effect on insulin sensitivity. Although this is the case, contrary to humans, fat mass is highly metabolically active in mice and is a substantial contributor of total glucose disposal and insulin dosage has been adjusted to total body weight as described in section “[Animals experiments](#)”. Further investigation on the tissue specific insulin sensitivity via the activation of its pathway would further deepen our understanding on the matter. Several mechanisms may underlie this:

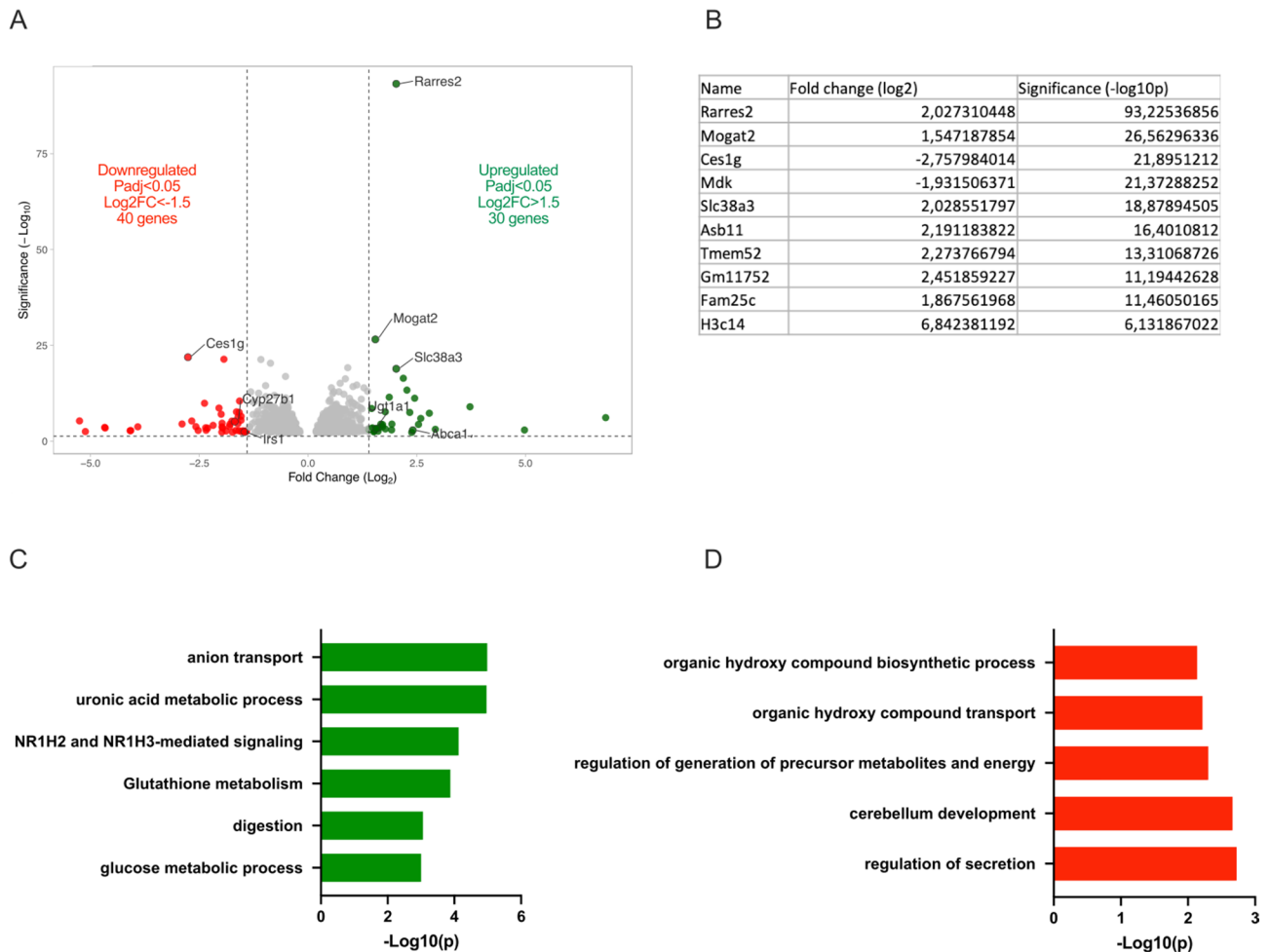


Fig. 7. Transcriptomic analysis in acidotic compared to control mice after 7 days of NH_4Cl treatment. **(A)** Volcano plot of the genes up- and down regulated by the treatment. **(B)** List of top 10 genes altered by metabolic acidosis. Functional enrichment of genes **(C)** upregulated and **(D)** downregulated by 7 days of NH_4Cl . Summary pathways analyzed by Metascape – $\log_{10}(p)$ values greater than 1,5 and less than –1,5 were selected with a False Discovery Rate (FDR) less than 0.05 and a p value less than 0.05.

(i) reduced hepatic and intestinal gluconeogenesis, (ii) glucosuria secondary to downregulation of SGLT's and (iii), increased renal glucose metabolism evidenced by elevated FDG uptake in the kidney and transcriptomic analysis. These findings challenge the classical view of acidosis as deleterious for glucose metabolism and suggest context-dependent benefits. Indeed, the mechanisms linking acute MA and alterations in insulin activity remain elusive. It is suggested that the acid-mediated inhibiting effects on insulin binding affinity to its receptor, on glycolysis, on the recycling of glucose transporters, and on insulin secretion may account for this phenomenon^{19–24,31–33}. In previous experiments, we found that treated mice who were given NH_4Cl for 16 h had similar glucose tolerance compared to their control (data not shown) whereas an increase was observed after 3 days and until 180 days. Data therefore suggest a biphasic response to acidosis between acute and chronic treatments.

Further mechanistic insights are provided as we showed that chronic MA regulates gluconeogenesis in a tissue-specific manner, resulting in a global reduction in fasting glucose. Total EGP induced by pyruvate was unchanged after 7 days, but was reduced in treated mice after 120 days, reinforcing the metabolic shift hypothesis. Reduced alanine stimulated EGP after 7 and 120 days suggests that chronic MA inhibits the hepatic gluconeogenic pathway, confirmed by the reduction Pck1 abundance observed in the liver^{33,34}. Acidosis has been shown to reduce the hepatic oxaloacetate (OAA) to malate ratio, limiting substrate availability for conversion to P-enolpyruvate by Pck1³³. Increased H^+ and NADH during acidosis may favor malate accumulation and OAA depletion via malate dehydrogenase^{2,35,36}. Chronic MA can therefore modulate hepatic TCA cycle flux and tissue specific EGP. Paradoxically, hepatic Pck1 knockout has been reported to increase total TCA flux, potentially contributing to the improved glucose tolerance observed in MA mice^{37,38}. These findings suggest that chronic MA downregulates hepatic gluconeogenesis by reducing Pck1 expression, potentially caused by an altered OAA/malate balance.

It is known that MA enhances glutamine metabolism by simultaneously generating glucose and ammonia to support systemic glucose supply while facilitating acid excretion³⁹. Renal Pck1 expression was consistently upregulated while G6pc was downregulated at later stages, suggesting that Pck1 expression during MA is crucial

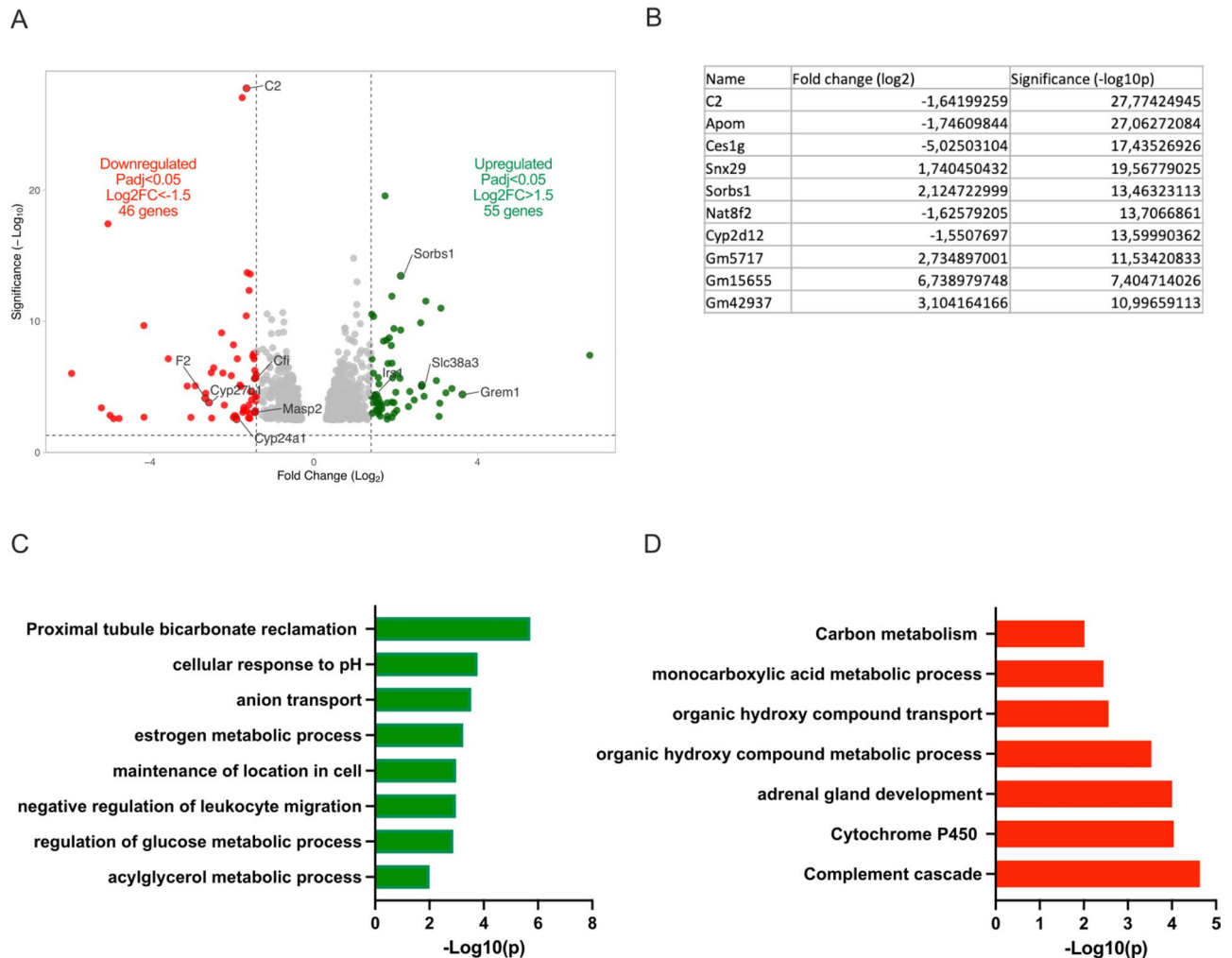


Fig. 8. Transcriptomic analysis in acidotic compared to control mice after 60 days of NH_4Cl treatment. **(A)** Volcano plot of the genes up- and down regulated by the treatment. **(B)** List of top 10 genes altered by metabolic acidosis. Functional enrichment of genes **(C)** upregulated and **(D)** downregulated by 60 days of NH_4Cl . Summary pathways analyzed by Metascape $-\log_{10}(p)$ values greater than 1.5 and less than -1.5 were selected with a False Discovery Rate (FDR) less than 0.05 and a p value less than 0.05.

to drive EGP production²⁵. We can therefore assume that the reduced glutamine induced EGP throughout our study is mainly due to a reduced duodenal and/or jejunal EGP. Indeed, glutamine fuels EGP in the kidney and small intestine (duodenum and jejunum), where the enzymatic machinery for glutamine catabolism is abundant, whereas the liver lacks glutaminase activity and instead relies predominantly on alanine and lactate⁴⁰. Although jejunal Pck1 protein abundance was unchanged in treated mice, G6pc seems to play a more decisive role in driving EGP in this tissue⁴¹.

It is important to keep in mind that glycogenolysis was not discussed in this paper, despite being an important part of EGP. Although this is the case, all pyruvate, glutamine and alanine tests have been done after 16 h fasts, which have shown to deplete almost entirely hepatic glycogen stores^{42,43}, showing a shift from glycogenolysis to gluconeogenesis over longer periods of fast. Further analysis on glycogenolysis and glycogen content would be needed to further deepen our understanding of the mechanisms by which acidosis improves glucose tolerance.

In parallel, MA reduced renal glucose reabsorption by downregulating *Sglt2* and *Sglt1* expression and reducing their protein abundance at later stages⁴⁴. This is not due to kidney damage as although glomerular filtration rate (GFR) was not measured, plasma creatinine concentration was similar between both groups and no histological alterations were observed (data not shown). Additionally, either a strong decrease in GFR or hyperglycemia could account for the glucosuria observed as early as 7 days after NH_4Cl loading, and neither were observed^{45,46}. RNA-seq revealed downregulation of *Hnf1a*, *Hnf4a*, and *NF- κ B* (via ubiquitin-dependent degradation of cyclin D^{47,48}), key transcriptional regulators of *Sglt1* and *Sglt2*^{49–54}, likely contributing to their reduced expression. These changes may confer renoprotection, as SGLT2 inhibition reduces ROS-related enzymes, including Nox2, Nox4, TGF- β 1, MCP-1, ICAM-1, and MPO^{55–57}, many of which were downregulated in NH_4Cl -treated kidneys. This was associated with significant glucosuria, a phenomenon reminiscent of pharmacological SGLT2 inhibition. Interestingly, *Glut2* expression was increased at later stages of the kinetic study, potentially as a compensatory

mechanism, to facilitate basolateral glucose export. These adaptations emphasize the kidney's central role in integrating glucose homeostasis with acid–base regulation. The glucosuria observed was measured prior and following a glucose oral bolus of 2 g/kg to challenge the renal glucose handling. This could be considered as a limitation as urine was not collected over 24 h in metabolic cages. Although this is the case, the aim of this experiment was to quantify the excretion of glucose with elevated glycemia to analyze if acidotic mice had a lower reabsorption threshold than their control, which is the case.

Transcriptomic analysis revealed broader metabolic adaptations. Genes involved in anion transport, bicarbonate reclamation, mitochondrial oxidative phosphorylation, and glucose and lipid metabolism were upregulated, consistent with renal metabolic reprogramming to support ammoniogenesis and maintain cellular energy^{58–66}. Functional studies are required to validate transcriptomic findings, as mRNA expression does not always reflect protein abundance⁶⁷. Time-course analysis demonstrated a biphasic transcriptional response: 156 genes were altered at day 3, with the number halving by day 7 and remaining stable thereafter, consistent with a transition from acute to chronic adaptation⁶⁸.

NH₄Cl supplementation has been classically used to induce MA in rodents, dogs and humans^{14–16,18,21,28,68}. Although the dehydration effects of NH₄Cl treatment remain controversial, we did not observe it in our study. Indeed, genes involved in osmotic regulation and water homeostasis such as aquaporin 2 and 3, the angiotensin 2 receptor, gremlin 2, the urea transporter, the vasopressin 2 receptor^{28,68,69} are not modified in the kidney of treated mice (data not shown). Additionally, male mice were used exclusively in this study to reduce variability associated with the estrous cycle in female mice, which can influence hormonal levels and potentially confound experimental outcomes.

Conclusion

Overall, our data show that, unlike acute acid–base disturbance, chronic MA improves glucose tolerance without changes in insulin sensitivity, likely due to reduced hepatic gluconeogenesis, decreased renal glucose reabsorption and increased energy demands in the kidney.

Material and methods

Ethical statements

Seven-week old male C57Bl/6Jrj mice were purchased from Janvier labs (Mayenne, France). *In vivo* experiments at Inserm 1283 – EGID, Université de Lille, Lille (France) were performed in compliance with the EU Directive 2010/63/EU for animal experiments Animal house agreements no. B 59-35010 (Authorization for Animal Experimentation no. 2020020516511947, Project approval by our local ethical committee no. CEEA 23998) and *in vivo* experiments at Inserm 1188 – Université de la Réunion, CYROI, Saint Clotilde, Reunion Island (France) were performed in compliance with the EU Directive 2010/63/EU for animal experiments Animal house agreements no. A 974 001 (Authorization for Animal Experimentation no. 201806111409218, Project approval by our local ethical committee no. CEEA 114). All methods are carried out in accordance with relevant guidelines and regulations and are reported in accordance with ARRIVE guidelines. At the time of euthanasia, the weight range of the mice was 28–40 g. All animals were euthanized either by cervical dislocation or cardiac puncture with Buprenorphine (0.05 mg/kg s.c.) and 4% isoflurane with a O₂ flux of 1 L/min for the initial anesthesia and 2% isoflurane with a O₂ flux of 0.5 L/min to maintain the anesthesia. All efforts were made to minimize suffering.

Animals experiments

Following the 10-day acclimatization, MA mice were given 0.28 M NH₄Cl (Sigma) in their sterile distilled drinking water. Control mice were given sterile distilled drinking water. Each mouse, as well as their food and liquid consumption, were weighted weekly. Experimental procedures took place after 3, 7, 14, 30, 60, 90, 150 and 180 days of NH₄Cl treatment. Metabolic phenotyping was performed as previously described^{25,70}. Briefly, intraperitoneal glucose (2 g of glucose per kg of body weight), insulin (0.75 U of insulin per kg of body weight), pyruvate (targeting global gluconeogenesis; 1 g of pyruvate per kg of body weight), alanine (targeting hepatic gluconeogenesis; 1 g of alanine per kg of body weight) and glutamine (targeting extra-hepatic gluconeogenesis; 1 g of glutamine per kg of body weight) tolerance tests were performed. All tests were done after a 16-h fast, except the ipITT which were done after a 6-h fast.

Glycemia was measured before and at different time after injections using the Accu-Check Performa (Roche Diagnostics) glucometer. Plasma insulin levels were measured using the mouse Insulin Elisa kit (Mercodia). Metabolic rate was measured by indirect calorimetry using the Phenomaster metabolic cage system (TSE Systems). Mice were housed individually and maintained at 21 °C under a 12 h light/12 h dark cycle. Food and water were available ad libitum. Lean, fat and fluid mass were measured using a Minispec LF50 (Bruker).

Sample analysis

Blood chemistry was measured using i-STAT EC8 + cartridge and i-STAT1 analyser (Abbott) on anesthetized animals using Buprenorphine (0.05 mg/kg s.c.) and 4% isoflurane with a O₂ flux of 1 L/min. Blood samples were taken by retro-orbital harvesting and used fresh at the time of the experiment. For urinary glucose concentration quantifications, mice were orally given 2 g/kg of glucose and urine collection was performed at T0 and T4h. Quantifications were done using a mouse glucose assay (ref: 81,692; Chrystal Chem) following manufacturer's instructions and normalized with creatinuria concentration. Urinary creatinine concentration was measured by ionic chromatography and spectrophotometry (235 nm).

Protein extracts and immunoblot analysis

Protein extraction and Western blots were carried out as previously described⁷¹. Tissues lysis was performed by using 150 mM NaCl, 1% Triton X-100; 50 mM Tris pH 7.8 and phosphatase (Roche) and protease inhibitors (Pierce) on ice. The renal plasma membrane-enriched fractions were prepared by differential centrifugation in 250 mM sucrose, 100 mM Tris-Hepes at pH 7.4 and phosphatase (Roche) and protease inhibitors (Pierce). Western blotting was performed using 15 µg for the kidney, liver and intestine lysates and 22.5 µg for the plasma membrane-enriched fractions of proteins loaded on SDS-PAGE precast gel (Biorad). The list of antibodies and the concentrations used are listed in Supplementary Table 1.

RNA expression and sequencing (RNA-seq)

Kidney and liver total RNA were extracted with the Rneasy lipid tissue (Qiagen) mini kit following manufacturer's instruction. qRT-PCR was carried out as previously described⁷⁰. Forward and reverse primers used are listed in Supplementary Table 2. RNA sequencing was done using the Kapa mRNA Hyperprep kit (Roche) in combination with the HiSeq 4000 sequencing system (Illumina). The demultiplexing of sequence data was performed using bcl2fastq Conversion Software (Illumina; bcl2fastq v2.20.0). Trimming of adapter sequences and low-quality reads was performed using trimmomatic software (version 0.39). Reads quality control was assessed using FastQC (v0.11.9). Subsequently, sequence reads from FASTQ files were aligned to the mouse genome (GRCm39), downloaded from GENCODE release M27. Alignment was performed using STAR aligner (version2.7.3a). On average, 20 millions of 75 base pairs paired-end reads were generated per sample. The normalized counts of the different genes and isoforms was performed using RSD (version 1.3.1) using a GTF from GENCODE M27 and EnSDbl 104 for gene name annotation. Finally, differential expression was performed using R version 3.6.3 and DESeq2 package v1.24.0. Four biological replicates *per* condition were used.

Glucose uptake via 2-deoxy-2-[18F] fluoroglucose

Mice were injected with 0.5 MBq/g of ¹⁸FDG and acquisition of positron emission tomography was assessed. Computed tomography (CT) scans were also acquired for anatomical landmarks and to obtain tissue attenuation coefficients necessary to correct the location of positrons emissions. Standard uptake values (SUV) were calculated using the total weight and the ¹⁸FDG dose injected to normalize the values. Zones were selected using the Statistical Parametric Map Inveon Research Workplace software (Version 4.2; Siemens Medical Solution).

Statistical analysis

Results were presented as mean ± SEM. Statistical analyses were performed using 2-Way ANOVA and subsequent Šidák testing for multiple comparison if the treatment condition was significant. Areas under the curve were analysed by unpaired *t*-test, if the *f*-test was statistically significant. In all analyses, *P* < 0.05 was considered statistically significant. *n* refers to the number of animals studied.

Data availability

The authors confirm that the data supporting the findings of this study are available within the article and its Supplementary material. Raw data that support the findings of this study are available from the corresponding author, upon reasonable request.

Received: 29 October 2025; Accepted: 28 January 2026

Published online: 03 February 2026

References

- Jager, K. J. et al. A single number for advocacy and communication-worldwide more than 850 million individuals have kidney diseases. *Nephrol. Dial. Transplant* **34** (11), 1803–1805 (2019).
- Burger, M. *Metabolic Acidosis* (StatPearls Publishing, 2023).
- Chan, J. Y. M., Islahudin, F., Tahir, N. A. M., Makmor-Bakry, M. & Tan, C. H. H. Prevalence, risk factors, and management of metabolic acidosis in chronic kidney disease patients: A multicenter retrospective study in Malaysia. *Cureus* **16** (3), e56314 (2024).
- Adamczak, M. et al. Diagnosis and treatment of metabolic acidosis in patients with chronic kidney disease - position statement of the working group of the polish society of nephrology. *Kidney Blood Press Res.* **43**, 959–962 (2018).
- Raphael, K. L. Metabolic acidosis in CKD: core curriculum. *Am. J. Kidney Dis.* **74**, 263–275 (2019).
- Souto, G., Donapetry, C., Calvino, J. & Adeva, M. M. Metabolic acidosis-induced insulin resistance and cardiovascular risk. *Metab. Syndr. Relat. Disord.* **9**, 247–253 (2011).
- Bellasi, A. et al. Correction of metabolic acidosis improves insulin resistance in chronic kidney disease. *BMC Nephrol.* **17** (1), 158 (2016).
- DiNicolantonio, J. J. & O'Keefe, J. H. Low-grade metabolic acidosis as a driver of insulin resistance. *Open Heart* **8** (2), (2021).
- Kim, H. J. Metabolic Acidosis in chronic kidney disease: pathogenesis, clinical consequences, and treatment. *Electrolyte Blood Press* **19** (2), 29–37 (2021).
- Kriz, W. & LeHir, M. Pathways to nephron loss starting from glomerular diseases-insights from animal models. *Kidney Int.* **67** (2), 404–419 (2005).
- Weiner, I. D. & Verlander, J. W. Renal ammonia metabolism and transport. *Compr. Physiol.* **3** (1), 201–220 (2013).
- Kraut, J. A. & Madias, N. E. Metabolic acidosis: pathophysiology, diagnosis and management. *Nat. Rev. Nephrol.* **6** (5), 274–285 (2010).
- Li, S. et al. Are low levels of serum bicarbonate associated with risk of progressing to impaired fasting glucose/diabetes? A single-centre prospective cohort study in Beijing, China. *BMJ Open* **8** (7), e019145 (2018).
- Mackler, B., Lichenstein, H. & Guest, G. M. Effects of ammonium chloride acidosis on glucose tolerance in dogs. *Am. J. Physiol.* **168** (1), 125–130 (1952).
- Guest, G., Mackler, B. & Knowles, H. J. Effects of acidosis on insulin action and on carbohydrate and mineral metabolism. *Diabetes* **1** (4), 276–282 (1952).
- Weisinger, J., Swenson, R., Greene, W., Taylor, J. & Reaven, G. Comparison of the effects of metabolic acidosis and acute uremia on carbohydrate tolerance. *Diabetes* **21** (11), 1109–1115 (1972).

17. Haldane, J. B. S., Wigglesworth, V. B. & Woodrow, C. The effect of reaction changes on human carbohydrate and oxygen metabolism. *Proc. R. Soc. London Ser. B, Containing Papers Biol. Charact.* **96** (672), 15–28 (1924).
18. DeFronzo, R. & Beckles, A. Glucose intolerance following chronic metabolic acidosis in man. *Am. J. Physiol.* **236** (4), 328–334 (1979).
19. Franch, H. A. et al. Acidosis impairs insulin receptor substrate-1-associated phosphoinositide 3-kinase signaling in muscle cells: consequences on proteolysis. *Am. J. Physiol. Renal Physiol.* **287** (4), F700–F706 (2004).
20. May, R., Masud, T., Logue, B., Bailey, J. & England, B. Chronic metabolic acidosis accelerates whole body proteolysis and oxidation in awake rats. *Kidney Int.* **41** (6), 1535–1542 (1992).
21. Whittaker, J., Cuthbert, C., Hammond, V. & Alberti, K. The effects of metabolic acidosis in vivo on insulin binding to isolated rat adipocytes. *Metabolism* **31** (6), 553–557 (1982).
22. Teta, D. et al. Acidosis downregulates leptin production from cultured adipocytes through a glucose transport-dependent post-transcriptional mechanism. *J. Am. Soc. Nephrol.* **14** (9), 2248–2254 (2003).
23. Dithabanchong, S. et al. Metabolic acidosis lowers circulating adiponectin through inhibition of adiponectin gene transcription. *Nephrol. Dial Transplant.* **26** (2), 592–598 (2011).
24. Igarashi, M. et al. Effect of acidosis on insulin binding and glucose uptake in isolated rat adipocytes. *Tohoku J. Exp. Med.* **169** (3), 205–213 (1993).
25. Mutel, E. et al. Control of blood glucose in the absence of hepatic glucose production during prolonged fasting in mice: induction of renal and intestinal gluconeogenesis by glucagon. *Diabetes* **60** (12), 3121–3131 (2011).
26. Ferrannini, E. Learning from glycosuria. *Diabetes* **60** (3), 695–696 (2011).
27. Johnsen, L. Ø., Sigad, A., Friis, K. A., Berg, P. M. & Damkier, H. H. NH₄Cl-induced metabolic acidosis increases the abundance of HCO₃⁻ transporters in the choroid plexus of mice. *Front Physiol* **15**, 1491793 (2024).
28. Nowik, M., Kampik, N. B., Mihailova, M., Eladari, D. & Wagner, C. A. Induction of metabolic acidosis with ammonium chloride (NH₄Cl) in mice and rats—species differences and technical considerations. *Cell Physiol. Biochem.* **26** (6), 1059–1072 (2010).
29. Fang, Y. W. et al. Chronic metabolic acidosis activates renal tubular sodium chloride cotransporter through angiotension II-dependent WNK4-SPAK phosphorylation pathway. *Sci. Rep.* **6**, 18360 (2016).
30. Mannon, E. C. et al. Renal mass reduction increases the response to exogenous insulin independent of acid-base status or plasma insulin levels in rats. *Am. J. Renal Physiol.* **321** (4), F494–F504 (2021).
31. Jakab, M. et al. The H⁺/K⁺ ATPase inhibitor SCH-28080 inhibits insulin secretion and induces cell death in INS-1E rat insulinoma cells. *Cell Physiol. Biochem.* **43** (3), 1037–1051 (2017).
32. Imenez Silva, P. H. & Mohebbi, N. Kidney metabolism and acid-base control: back to the basics. *Pflugers Arch.* **474** (8), 919–934 (2022).
33. Iles, R., Cohen, R., Rist, A. & Baron, P. The mechanism of inhibition by acidosis of gluconeogenesis from lactate in rat liver. *Biochem. J.* **164** (1), 185–191 (1977).
34. Beech, J., Iles, R. & Cohen, R. Bicarbonate in the treatment of metabolic acidosis: effects on hepatic intracellular pH, gluconeogenesis, and lactate disposal in rats. *Metabolism* **42** (3), 341–346 (1993).
35. Minarik, P., Tomaskova, N., Kollarova, M. & Antalík, M. Malate dehydrogenases—structure and function. *Gen. Physiol. Biophys.* **21** (3), 257–265 (2002).
36. Aamer, E. et al. Influence of electrode potential, pH and NAD(+) concentration on the electrochemical NADH regeneration. *Sci. Rep.* **12** (1), 16380 (2022).
37. She, P. et al. Mechanisms by which liver-specific PEPCK knockout mice preserve euglycemia during starvation. *Diabetes* **52** (7), 1649–1654 (2003).
38. Burgess, S. et al. Impaired tricarboxylic acid cycle activity in mouse livers lacking cytosolic phosphoenolpyruvate carboxykinase. *J. Biol. Chem.* **279** (47), 48941–48949 (2004).
39. Baldini, N. & Avnet, S. The effects of systemic and local acidosis on insulin resistance and signaling. *Int. J. Mol. Sci.* **20** (1), 126 (2019).
40. Holeček, M. Origin and roles of alanine and glutamine in gluconeogenesis in the liver, kidneys, and small intestine under physiological and pathological conditions. *Int. J. Mol. Sci.* **25** (13), 7037 (2024).
41. Mithieux, G., Rajas, F. & Gautier-Stein, A. A novel role for glucose 6-phosphatase in the small intestine in the control of glucose homeostasis. *J. Biol. Chem.* **279** (43), 44231–44234 (2004).
42. Fu, J., Liu, S. & Li, M. Optimal fasting duration for mice as assessed by metabolic status. *Sci. Rep.* **14**, 21509 (2024).
43. Carper, D., Coué, M., Laurens, C., Langin, D. & Moro, C. Reappraisal of the optimal fasting time for insulin tolerance tests in mice. *Mol. Metab.* **42**, 101058 (2020).
44. Lee, Y., Lee, Y. & Han, H. Regulatory mechanisms of Na⁽⁺⁾/glucose cotransporters in renal proximal tubule cells. *Kidney Int. Suppl.* **72** (106), S27–S35 (2007).
45. Liman, M. N. P. & Jialal, I. *Physiology, Glycosuria* (StatPearls Publishing, 2023).
46. Zhang, J. et al. Macula densa SGLT1-NOS1-tubuloglomerular feedback pathway, a new mechanism for glomerular hyperfiltration during hyperglycemia. *J. Am. Soc. Nephrol.* **30** (4), 578–593 (2019).
47. Caudron-Herger, M. & Diederichs, S. 2021 Insights from the degradation mechanism of cyclin D into targeted therapy of the cancer cell cycle. *Signal Transduct. Target Ther.* **6** (1), 311 (2021).
48. Guo, Z. Y. et al. The elements of human cyclin D1 promoter and regulation involved. *Clin. Epigenet.* **2** (2), 63–76 (2011).
49. Pontoglio, M. et al. HNF1 α controls renal glucose reabsorption in mouse and man. *EMBO Rep.* **1** (4), 359–365 (2000).
50. Freitas, H. et al. Na⁽⁺⁾-glucose transporter-2 messenger ribonucleic acid expression in kidney of diabetic rats correlates with glycemic levels: involvement of hepatocyte nuclear factor-1 α expression and activity. *Endocrinology* **149** (2), 717–724 (2008).
51. Takesue, H., Hirota, T., Tachimura, M., Tokashiki, A. & Ieiri, I. Nucleosome positioning and gene regulation of the SGLT2 gene in the renal proximal tubular epithelial cells. *Mol. Pharmacol.* **94** (3), 953–962 (2018).
52. Bonner, C. et al. Inhibition of the glucose transporter SGLT2 with dapagliflozin in pancreatic alpha cells triggers glucagon secretion. *Nat. Med.* **21** (5), 512–517 (2015).
53. Marable, S. S., Chung, E. & Park, J.-S. Hnf4a is required for the development of Cdh6-expressing progenitors into proximal tubules in the mouse kidney. *J. Am. Soc. Nephrol.* **31** (11), 2543–2558 (2020).
54. Fu, M. et al. Epoxyeicosatrienoic acids improve glucose homeostasis by preventing NF- κ B-mediated transcription of SGLT2 in renal tubular epithelial cells. *Mol. Cell Endocrinol.* **523**, 111149 (2021).
55. Tang, L. et al. Dapagliflozin slows the progression of the renal and liver fibrosis associated with type 2 diabetes. *Am. J. Physiol. Endocrinol. Metab.* **313** (5), E563–E576 (2017).
56. Terami, N. et al. Long-term treatment with the sodium glucose cotransporter 2 inhibitor, dapagliflozin, ameliorates glucose homeostasis and diabetic nephropathy in db/db mice. *PLoS ONE* **9** (6), e100777 (2014).
57. Yao, D., Wang, S., Wang, M. & Lu, W. Renoprotection of dapagliflozin in human renal proximal tubular cells via the inhibition of the high mobility group box 1-receptor for advanced glycation end products-nuclear factor- κ B signaling pathway. *Mol. Med. Rep.* **18** (4), 3625–3630 (2018).
58. Faivre, A., Verissimo, T., Auwerx, H., Legouis, D. & de Seigneux, S. Tubular cell glucose metabolism shift during acute and chronic injuries. *Front Med (Lausanne)* **8**, 742072 (2021).
59. Gao, Y., Nelson, D. W., Banh, T., Yen, M. I. & Yen, C. L. E. Intestine-specific expression of MOGAT2 partially restores metabolic efficiency in Mogat2-deficient mice. *J. Lipid Res.* **54** (6), 1644–1652 (2013).

60. Lin, P. H. & Duann, P. Dyslipidemia in kidney disorders: perspectives on mitochondria homeostasis and therapeutic opportunities. *Front. Physiol.* **11**, 1050 (2020).
61. Sanz, A. B. et al. NF-kappaB in renal inflammation. *J. Am. Soc. Nephrol.* **21** (8), 1254–1262 (2010).
62. Verissimo, T. et al. PCK1 is a key regulator of metabolic and mitochondrial functions in renal tubular cells. *Am. J. Physiol. Renal Physiol.* **324** (6), F532–F543 (2023).
63. Wang, G. et al. Fat storage-inducing transmembrane proteins: beyond mediating lipid droplet formation. *Cell Mol. Biol. Lett.* **27** (1), 98 (2022).
64. Bhargava, P. & Schnellmann, R. G. Mitochondrial energetics in the kidney. *Nat. Rev. Nephrol.* **13** (10), 629–646 (2017).
65. Gumz, M. L., Lynch, I. J., Greenlee, M. M., Cain, B. D. & Wingo, C. S. The renal H⁺-K⁺-ATPases: physiology, regulation, and structure. *Am. J. Physiol. Renal Physiol.* **298** (1), F12–21 (2010).
66. Zhao, L. et al. Energy metabolic reprogramming regulates programmed cell death of renal tubular epithelial cells and might serve as a new therapeutic target for acute kidney injury. *Front. Cell Dev. Biol.* **11**, 1276217 (2023).
67. Greenbaum, D., Colangelo, C., Williams, K. & Gerstein, M. Comparing protein abundance and mRNA expression levels on a genomic scale. *Genome Biol.* **4** (9), 117 (2003).
68. Nowik, M. et al. Genome-wide gene expression profiling reveals renal genes regulated during metabolic acidosis. *Physiol. Genom.* **32** (3), 322–334 (2008).
69. Huynh, N. V., Rehage, C. & Hyndman, K. A. Mild dehydration effects on the murine kidney single-nucleus transcriptome and chromatin accessibility. *Am. J. Physiol. Renal Physiol.* **325** (6), F717–F732 (2023).
70. Annicotte, J. S. et al. The CDK4-pRB-E2F1 pathway controls insulin secretion. *Nat. Cell Biol.* **11** (8), 1017–1023 (2009).
71. Lopez-Cayuqueo, K. I. et al. A mouse model of pseudohypoaldosteronism type II reveals a novel mechanism of renal tubular acidosis. *Kidney Int.* **94** (3), 514–523 (2018).

Acknowledgements

The authors thank the Experimental Resources platform from Lille University, especially CDegraeve, JVerboten, RDehaynin and JDevassine for animal care. We also thank LPinot, and SMEulebrouck for helpful discussions and technical assistance. We would also like to thank Dr Gilles Mithieux and Dr Fabienne Rajas for the anti-G6PC antibody kindly gifted under the Open Material Transfer Agreement (MTA) regulations.

Author contributions

NZ, JB-V and RC conceptualized the study. NZ, JMontaigne, JMerrheim, CD, EC, FA, JB-V, ED, BT and RC performed the investigations. NZ, SA and MD did the formal analyses and data curation. EC, BS, PF, AB and RC contributed to resources. NZ, AB and RC contributed to data visualization. NZ, CB and AB wrote the first draft. NZ and CB supervised the conception of the article. All authors revised the manuscript for intellectual content, and read and approved the final manuscript.

Funding

This work was supported by grants from the French National Research Agency: ANR-16-CE14-0031 to RC, from the Association pour l'utilisation du rein artificiel à la Réunion (AURAR)-Philancia to RC, from the Soutien à l'accueil de Talents de la Recherche Scientifique (STaRS), Région Hauts-de-France to RC, the French National Research Agency (ANR-10-LABX-46 [European Genomics Institute for Diabetes] to PF and AB and ANR-10-EQPX-07-01 [LIGAN-PM]) to PF and AB, and from the National Center for Precision Diabetic Medicine – PreciDIAB, which is jointly supported by the French National Agency for Research (ANR-18-IBHU-0001) to PF and AB, by the European Union (FEDER), by the Hauts-de-France Regional Council and by the European Metropolis of Lille (MEL). AB holds an ERC consolidator grant (OpiO, contract number 101043671).

Declarations

Competing interests

The authors declare no competing interests.

Additional information

Supplementary Information The online version contains supplementary material available at <https://doi.org/10.1038/s41598-026-38007-7>.

Correspondence and requests for materials should be addressed to N.Z. or C.B.

Reprints and permissions information is available at www.nature.com/reprints.

Publisher's note Springer Nature remains neutral with regard to jurisdictional claims in published maps and institutional affiliations.

Open Access This article is licensed under a Creative Commons Attribution 4.0 International License, which permits use, sharing, adaptation, distribution and reproduction in any medium or format, as long as you give appropriate credit to the original author(s) and the source, provide a link to the Creative Commons licence, and indicate if changes were made. The images or other third party material in this article are included in the article's Creative Commons licence, unless indicated otherwise in a credit line to the material. If material is not included in the article's Creative Commons licence and your intended use is not permitted by statutory regulation or exceeds the permitted use, you will need to obtain permission directly from the copyright holder. To view a copy of this licence, visit <http://creativecommons.org/licenses/by/4.0/>.

© The Author(s) 2026